

# New results from the technological prototype of the CALICE highly-granular silicon tungsten electromagnetic calorimeter

V. Boudry for the CALICE collaboration<sup>1\*</sup>

arXiv:2211.05614v1 [hep-ex] 10 Nov 2022

## Abstract

An extended version of the CALICE silicon-tungsten ECAL was tested in November 2021 at the DESY beam test facility. With 15 active layers, it featured some with a thin PCB design, and a new compact DAQ system handling all layers in a common set. The noise, self-trigger performances and response to punch-through electrons, without tungsten absorbers, have been evaluated for each of the 15360 channels, using an improved procedure. Showers of low-energy electrons (1 to 6 GeV) have been recorded in two configurations of absorber, and are being analysed. Some preliminary results at the cell level will be presented.

## Keywords

Calorimetry, Higgs Factory, Granularity, Beamtest

<sup>1</sup>Laboratoire Leprince-Ringuet, CNRS, École polytechnique, Institut Polytechnique de Paris, 91120 Palaiseau, France.

\*Corresponding author: vincent.boudry@in2p3.fr

## Contents

<b>1</b>	<b>Introduction</b>	<b>1</b>
1.1	Particle Flow Detectors at Higgs Factories . . . . .	1
1.2	An Ultra-Granular SiW-ECAL for Higgs Factories	1
1.3	CALICE prototypes for ILC . . . . .	2
<b>2</b>	<b>Data taking at the DESY beam test facility</b>	<b>3</b>
2.1	Beam characteristics . . . . .	3
2.2	Prototype layouts . . . . .	3
<b>3</b>	<b>Noise studies</b>	<b>3</b>
<b>4</b>	<b>Response to MIPs</b>	<b>3</b>
<b>5</b>	<b>Response to low-energy electrons</b>	<b>4</b>
5.1	Simulation . . . . .	4
5.2	In-shower cell energy spectrum . . . . .	4
<b>6</b>	<b>Outlook</b>	<b>4</b>
<b>7</b>	<b>Acknowledgements</b>	<b>5</b>
	<b>References</b>	<b>5</b>

## 1. Introduction

### 1.1 Particle Flow Detectors at Higgs Factories

Detectors for future Higgs factories, near any  $e^+e^-$  colliders (ILC, FCC-ee, CEPC, CLIC) will require an excellent energy resolution for jets, particle identification and a large acceptance. Highly-granular calorimeters, and especially electromagnetic ones (ECAL), are requested by Particle Flow Algorithms (PFA): with a track momentum resolution of  $\delta p/p \sim 5 \cdot 10^{-5}$  the charged particles below few hundreds of

GeV are better reconstructed with the tracker; calorimetric uncertainties at low energy are then confined to neutral particles, for 25% (in jet energy fraction) in photons and 10% in neutral hadrons (2/3 of which will start interacting in the ECAL). The imaging capacity of the calorimeters is critical to separate neutral from charged showers.

Particle identification can also exploit the shower shapes, and by time-of-flight in the ECAL complements the tracker  $dE/dx$  at low momentum. A precision timing of a few 10's of ps is linked to the small cell size (30ps  $\sim$  1cm/c) in those devices.

### 1.2 An Ultra-Granular SiW-ECAL for Higgs Factories

The requirements of imaging capabilities for an ECAL add to the standard ones (hermeticity, linearity, stability, and uniformity in position and angle), the handling of a very large number of channels, and the need to have compact devices to better separate nearby particles. The ECAL must also have a large dynamic range at the cell level, to detect and track particles at their minimum of ionization (1 MIP or about 4fC) and measure electrons and photons of a 100's of GeV (2000 MIPs).

Highly resistive Silicon sensors made of large area segmented PIN diodes fulfil all the listed requirements (flexibility in the design, sensitivity, stability, speed), at a cost slightly larger than other solutions, but providing also an intrinsic stability of calibration and linearity. Associated with tungsten as absorber and a carbon fibre holding structure, the silicon-tungsten ECAL (SiW-ECAL) offers compactness and uniformity by minimizing dead spaces.

For a SiW-ECAL at the ILC, for which this R&D was initi-

ated, an optimal configuration was found [1] in having 55 mm<sup>2</sup> cells and 30 layers in depth, for 24 X<sub>0</sub> and 500 μm-thick sensors. Having a channel density of ~ 600 channel/dm<sup>3</sup>, and a 100 million channels, imposes to have readout ASICs integrated in detector, with a low power consumption. Their support boards connecting them to the sensors, must be designed in the perspective of the production of 100,000's of elements. The full design of the SiW-CAL is described in [2] and [3].

### 1.3 CALICE prototypes for ILC

The CALICE collaboration aims at developing and testing imaging calorimeters for the Higgs Factories.

A so-called SiW-ECAL “physics prototype” was built and tested from 2005 to 2011. It featured 6 cm-wide, 500 μm-thick silicon sensors, subdivided in 11 cm<sup>2</sup> cells, over an active surface of 2424 cm<sup>2</sup>, for 30 layers. The cells were glued to pads on the readout PCB, and the signal collected by external electronics. This device provided a proof-of-principle for this kind of design, but lacked many of the technological constraints listed previously.

Since 2010, a “technological prototype” is on the making which is the subject of this contribution. Its base unit is called an ASU (Assembly Single Unit), made of a front-end board (FEV), hosting 16 readout ASICs, the SKIROC2, and onto which 4 silicon sensors are glued. The channel density has then increased by a factor 4, with cells sizes of 55 mm<sup>2</sup>, and the square silicon diode matrices enlarged to 99 cm<sup>2</sup>. Overall, 22 ASUs have been produced with different FEV designs and sensor thicknesses, out of which 15 have been stacked to form a 1818 cm<sup>2</sup> calorimeter. This contribution summarizes some preliminary results obtained using this device.

A complementary important milestone will be chaining of 8 ASUs into a long cassette, the detector base element for a large SiW-ECAL, not described here [4].

**The SKIROC2 ASIC** Designed by the Omega lab [5] for a SiW-ECAL at the ILC, it pioneered the embedded readout of highly-granular electromagnetic silicon calorimeters<sup>1</sup>. The signal of each of the 64 channels is pre-amplified and sent to 3 branches: one with a fast shaping (~ 20 ns) for triggering and timing purposes, and two with slow shapers (~ 200 ns) for amplitude measurements, using gains of 1 and 10 respectively.

When a signal of any channel is over the threshold, the amplitudes of the 642 slow shapers are stored. At the end of an acquisition period, the 215 analogue memories per channels are converted using 12-bit Wilkinson ADCs, and tagged with a “Bunch-crossing” ID (BCID), counting the periods spent between the spill start and the trigger.

**The integration challenge** In the final detector, cassettes of 8 to 12 ASUs, for 1.6 to 2.2 m long, must be operated from a single end, to ensure the detector uniformity. Most of the technological constraints concentrate on the FEV design.

The FEV ensures power distribution, clock and configuration dispatching to the ASICs, and their data collection, using daisy-chaining to minimize the number of transmissions lines (140 at this time). This must be done without compromising the weak signal (2 fC to 10 pC) transmission from the sensors to the ASIC. Additionally, the FEV thickness must be kept low, of the order of 2 mm, ASIC and ancillary electronics included, in order to keep the detector compact. A lateral mechanical precision of ~ 50 μm is requested to keep the ASUs properly aligned, and to protect the sensors while minimizing the gaps between the ASUs. The flatness of the FEVs is also checked, to avoid stressing the sensors glued to them. Finally, a specific R&D towards reliable low-profile connectors was realized.

The FEVs currently used in the prototype come in two flavours:

- BGA: one in which the ASICs are packaged, using Ball Grid Array (BGA) connection. This allows for pre-mounting testing of the ASICs and an easier handling, at the expense of the thickness: ~ 1.2 mm are needed, which is also used for connectors, filters, etc. Versions FEV10 to FEV13 of these boards are in use. They were equipped with sensors of 320, 500 and 650 μm.
- COB The original design embeds the naked ASICs inside the PCB, with a direct bonding connection, are dubbed COB (for Chip-in-Board). The additional difficulties (mechanical constraint, absence of decoupling) are just being lifted. The first two working versions of the COBs, based one FEV11, have been employed. They are mostly equipped of 500 μm sensors.

**A compact DAQ** For the final detector a space of only ~ 3 cm is foreseen between the Hadronic Calorimeter and the ECAL. All services (power, cooling, DAQ, mechanical support) must take place in this space, at one end of the cassettes.

A new DAQ system has lately been put in production; 15 layers, connected through their interface board (SLBoard), can be operated by a mezzanine board on a CORE module, via a single thin Kapton (see Fig 1). It has been designed as a prototype of the final DAQ electronics [6]. The SLBoard ensures low- and high-voltage powering, DAQ clock and control distribution. It presents a longitudinal span of less than 6 cm, close to the design of 4.3 cm (3 cm/cos(45)), a height compatible with a layer spacing of 15 mm, and leaves space for the active cooling pipe at the centre.

A labWindows-based acquisition and monitoring application controls and read the CORE module via a single USB2 cable. The data can be partially analysed online to provide basic or advanced distributions (number of hits per layer, hit maps, amplitude and time distribution...) for optimal or reduced acquisition speeds. An interface to the EUDAQ software developed for AIDA & AIDA-2020 [7], is provided; it allows for combined running with other compatible devices, such as the EUDET/AIDA telescope, the CALICE AHCAL,

...

<sup>1</sup>it was used for the early prototype of HGCAL, then derived as SKIROC-CMS, and finally fully redesigned as HGCROC.

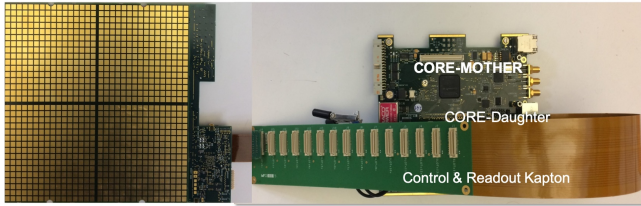


**Figure 1.** Picture of the complete DAQ attached to a single layer.

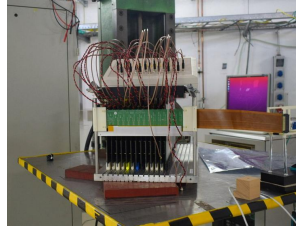


**Figure 2.** Left) Back of a detection layer, consisting of one ASU connected to a SLBoard. It is mounted on a 2 mm Carbon plate, equipped with 3D-printed rail supports. The associated tungsten plate can be mounted on the other side of the carbon plate. Right) The hosting case, stripped of its lateral plates, with 15 layers, a CORE Kapton connector, and the electric patch panel (top) distributing the low- and high-voltages.

## 2. Data taking at the DESY beam test facility

### 2.1 Beam characteristics

The DESY beam test facility [8] offers beam of electrons or positrons, of 1 to 6 GeV, with a peak intensity around 3 GeV at a few kHz. The beam spot on the detector had a Gaussian profile of about 10 mm.

Four weeks of tests have been used in November 2021 and March 2022. About three weeks were dedicated to the commissioning and training of the system, adjusting detector electronics and DAQ parameters, calibration and monitoring tools.

### 2.2 Prototype layouts

During this campaign, 15 detection layers (see 2left) were operated together for the first time, in a calorimeter configuration. The detection layers are mounted in a protective case (see 2right), providing a constant spacing of 15 mm, lateral alignment and light and electromagnetic protection.

Three tungsten absorber configurations have been employed, with (seen from the beam entrance):

**noW** no tungsten;

**TB2021** 11 layers of 2.1 mm ( $0.6 X_0$ ) plus 3 layers of 4.2 mm ( $1.2 X_0$ ) for  $10.2 X_0$  in total;

**TB2022** 7 layers of 2.8 mm ( $0.8 X_0$ ) plus 8 layers of 4.2 mm ( $1.2 X_0$ ) for  $15.2 X_0$  in total.

The first configuration (“noW”) lets the electrons pass almost unhindered, providing a pseudo MIP signal. The second and third configurations were used in November 2021 and March 2022.

## 3. Noise studies

The low occupancy of highly-granular calorimeters operated at lepton colliders allows for local triggering. For pulsed, linear colliders (not so for continuous, circular colliders), the data can be locally stored until the end of a bunch spill, and converted and readout outside the acquisition period. This operating mode allows to reduce the power consumption, but renders the electronics highly sensitive to noisy channels and collective modes, which can fill the local memories, effectively blinding the ASICs. A careful tuning of the threshold (common to all channels in the SKIROC2), and masking of the noisier channels is mandatory, and can only be done in beam<sup>2</sup>.

The partial zero-suppression of the SKIROC2, where a single ‘hit’, defined as a channel above threshold, triggers the readout of all channels, ensures the recording of many noise signal in both high and low-gain branches. These were analysed in terms of coherent and incoherent sources, using the framework of [9]: assuming Gaussian noise sources, the inter-channel correlation allows quantifying the different contributions. The 230,400 memories cells have been analysed, the pedestal and incoherent noise extracted (see fig 3 for the high-gain branch.). The pedestal distribution exhibits primarily a per-chip correlation, due to the ASICs technological analogue dispersion. Using a pre-amplifier feedback capacitance of 0.8 pF, the incoherent noise is found in the 2.5 to 3.5 ADC-count range, depending essentially on the wafer thickness. This must be compared to the signal of a MIP, ranging between 70 and 140 ADC-counts for 320 and 650  $\mu\text{m}$  sensors respectively<sup>3</sup>, and is similar to previous results using individual fitting of the channels [10]. The noise pattern is now well identified, with a clear influence of power lines near the SLBoard, a recurring problematic channel number (37) on all ASICs, occasionally affecting its neighbours, plus some random rogue ones. The FEV13 design tackled most of the issues (but channel 37).

## 4. Response to MIPs

The inter-calibration is performed by a positional scan with all the tungsten removed (“noW”). The observed spectra in very cell can be nicely be fitted by a Landau convoluted with a Gaussian. Simulation studies have shown no obvious difference in MIP spectrum stemming from a 3 GeV electron and a muon, but for the presence of a small second MIP peak in the last layers.

<sup>2</sup>the signal-to-noise ratio is vastly different in cosmics and beam operations, especially due to pulsing operation.

<sup>3</sup>this translates to SNR of 20 to 40 for that branch.

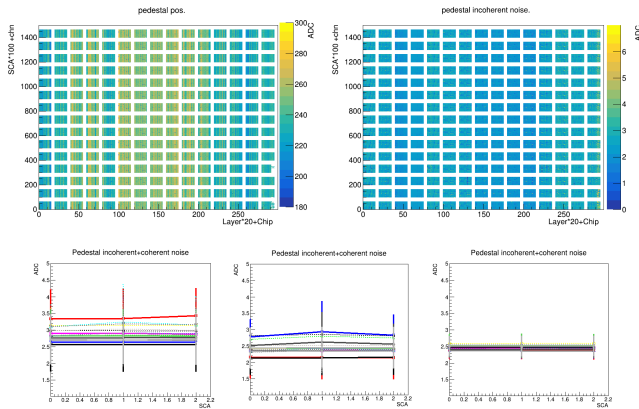


**Figure 3.** Top) Pedestal (left) and incoherent noise (right) in units of ADC counts for each of the 230,400 memory cells. Bottom) Average and dispersion of incoherent noise measurements on the 64 channels, for the 3 first memories, for each of the 16 ASIC of 3 types of boards: COP (left), FEV12 (middle), FEV13 (right). Compared to the FEV12, the COB suffers slightly from the near lack of decoupling capacitors. The optimization of signal routing on the FEV13, based on observations on the previous versions, is clearly visible.

The overall picture shows a very uniform response in many layers, in perfect correlation with the thickness of sensors. But some layers feature a pattern of missing signal (statistics too low to perform fits) at the edge of some sensors. The pattern suggests a weakness of the conductive glue dots connecting the sensors to the FEV’s readout pads, which is under investigation.

## 5. Response to low-energy electrons

### 5.1 Simulation

A detailed simulation of the prototype has been done using GEANT4, the geometry being described by the DD4HEP framework. A digitization module mimicking the processing signal by the SKIROC2 is being tuned on this set of data. The cells masked during the acquisition are also masked in the simulated data.

### 5.2 In-shower cell energy spectrum

The energy deposited in 3 types of boards by 3 GeV electron showers are displayed in figure 4.

The contributions from singles, pairs or triplets of particles can be clearly separated in the FEV13-based ASU, placed at the front of the calorimeter, after  $1.6X_0$ . This is well reproduced by the raw simulation (no digitization applied). It can be observed that the noise contribution, which should enlarge the peaks, is small. The effective threshold can be determined, at a value of about  $1/4^{\text{th}}$  of a the most probable value (MPV) of a MIP, with a small dispersion.

At the place of the COB-based ASU, placed at  $3.2X_0$  from the front, only the single particles and pairs can be seen.

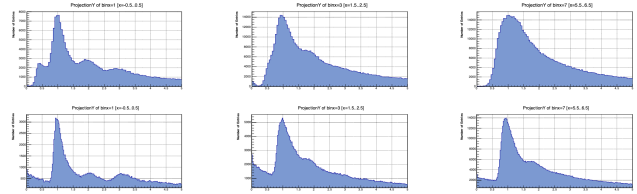


**Figure 4.** Energies deposited in cells of an FEV13 equipped with  $650\ \mu\text{m}$  sensors (left), a COB with  $500\ \mu\text{m}$  sensors (middle) and a FEV11 with  $320\ \mu\text{m}$  sensors, scaled to the Most Probable Value for a single particle crossing the cell, by 3 GeV electrons using the TB2022 configuration. On top the spectra from data, at the bottom simulated ones, without digitization.

A threshold can be estimated around  $1/2.5^{\text{th}}$  of the MPV.

Past the maximum of the shower ( $6.8X_0$ ), the single- and two-particle peaks are still visible in the simulated data, but are washed out by the noise on the FEV11-based ASU. Here, the identification of the main peak is unclear: it could be a single-particle with washed-out 2-particle peak, or the 2-particle peak, with the single-particle one cut-out by the electronics threshold. Only the comparison with neighbouring layers and scaling allows deciding for the first hypothesis. An effective threshold around  $1/1.5^{\text{th}}$  of the MPV can be estimated, cutting part of the foot of first peak.

Provided a sufficient signal-to-noise ratio, in-shower calibration of the response to a MIP and position of the threshold can thus be performed.

A saturation of the spectra of the cell energy in the high-gain branch has been observed in the ASUs equipped with  $500\ \mu\text{m}$  or  $650\ \mu\text{m}$  sensors for 3 GeV electrons. Linearity is kept in the low-gain branch even for the 6 GeV, but the gain must be adjusted for higher beam energy such as the one at CERN facility. Configuring a higher feedback capacitor in the SKIROC2 pre-amplification (6 pF instead of 0.8 or 1.2 pF), yielded a ratio of 4.73 between the two gains, extracted from MIP calibration.

## 6. Outlook

The data set recorded at the DESY beam test facility in November 2021 and March 2022, with the first version of the SiW-ECAL prototype featuring enough layers to perform a quantitative analysis of its calorimetric response are being analysed. Noise and punch-through electrons have yielded calibrations for the equalization of detector response and masking of defective channels. The detector is mostly performing as expected, with per-layer calibration sets compatible with the previous campaigns. But weaknesses in the gluing dots near some sensor edges have been observed.

The estimations of the energy resolution will require full calibration and the proper handling of the detectors features (e.g. masked channels).

The electrons shower’s per-cell energy deposition is roughly

reproduced by the simulation; this will be refined by tuning and applying the digitization mimicking the SKIROC2 signal processing. For layers with a proper signal-to-noise ratio, energy calibration and threshold value of individual cells can be extracted directly from the shower data.

The highest possible electronics gain, used so far to study the noise and low-energy response, saturates part of the read-out event in 3 GeV electron showers. For the next campaign at CERN in June 2022, this gain will be reduced, more FEV13-based ASU will replace ageing FEV11-based ones, and more tungsten to better contain high-energy electron showers.

Finally, the behaviour of existing layers has provided input to correct the design of the next generation of boards, to be produced by the end of 2022, improving on power and signal distribution, stabilization, flexibility and HV filtering.

## 7. Acknowledgements

This project has received funding from the European Union's Horizon 2020 research and innovation programme under grant agreement No 101004761. The measurements leading to these results have been performed at the Test Beam Facility at DESY Hamburg (Germany), a member of the Helmholtz Association (HGF).

## References

- [1] M. A. Thomson, “Particle Flow Calorimetry and the PandoraPFA Algorithm,” *Nucl. Instrum. Meth.* **A611** (2009) 25–40.
- [2] T. Behnke *et al.*, “The International Linear Collider Technical Design Report - Volume 4: Detectors,” *ArXiv13066329 Phys.* (June, 2013), arXiv:1306.6329 [physics].
- [3] The ILD Collaboration, “International Large Detector: Interim Design Report,” *ArXiv200301116 Hep-Ex Physicsphysics* (Mar., 2020), arXiv:2003.01116 [hep-ex, physics:physics].
- [4] F. Magniette *et al.*, “ILD Silicon Tungsten Electromagnetic Calorimeter First Full Scale Electronic Prototype,”.
- [5] T. Suehara *et al.*, “Performance Study of SKIROC2/A ASIC for ILD Si-W ECAL,” *ArXiv180102024 Phys.* (Jan., 2018), arXiv:1801.02024 [physics].
- [6] D. Breton *et al.*, “CALICE SiW ECAL - Development and Performance of a Highly Compact Digital Readout System,” *JINST* **15** no. 05, (2020) C05074.
- [7] Y. Liu *et al.*, “EUDAQ2—A flexible data acquisition software framework for common test beams,” *JINST* **14** no. 10, (2019) P10033, arXiv:1907.10600 [physics.ins-det].
- [8] R. Diener *et al.*, “The DESY II Test Beam Facility,” *NIM A* **922** (Apr., 2019) 265–286.
- [9] T. Frisson and R. Poeschl, “Coherent Noise Source Identification in Multi Channel Analysis,” arXiv:1401.7095 [hep-ex, physics:physics].
- [10] K. Kawagoe *et al.*, “Beam test performance of the highly granular SiW-ECAL technological prototype for the ILC,” *Nucl. Instrum. Meth. A* **950** (2020) 162969, arXiv:1902.00110 [physics.ins-det].